

Reversible Hydrogen Bond Network Dynamics: Molecular Dynamics Simulations of Calix[4]arene-Catenanes

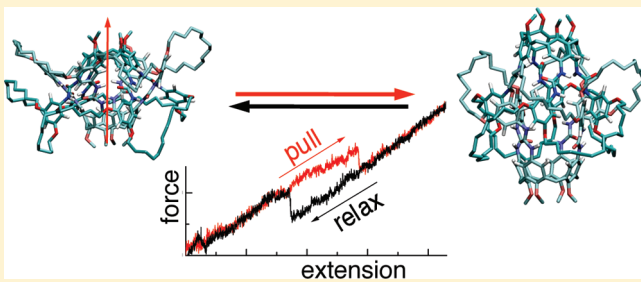
Thomas Schlesier,[†] Thorsten Metzroth,[†] Andreas Janshoff,[‡] Jürgen Gauss,[†] and Gregor Diezemann^{*,†}

[†]Institut für Physikalische Chemie, Universität Mainz, Jakob-Welder-Weg 11, 55128 Mainz, Germany

[‡]Institut für Physikalische Chemie, Universität Göttingen, Tammannstrasse 6, 37077 Göttingen, Germany

 Supporting Information

ABSTRACT: We present detailed molecular dynamics (MD) simulations of mechanically interlocked calix[4]arene-catenanes under external force. Single-molecule force spectroscopy experiments revealed that the separation of dimers with two aliphatic loops results in reversible hydrogen bond breakage through an intermediate in a triple-well potential, while the tetra-loop species separates in a one-step manner (Janke, M.; et al. *Nat. Nanotechnol.* 2009, 4, 225). MD simulations show that calix[4]arenes interlocked by four loops (**1**) display a complete restructuring of the hydrogen bond network under mechanical force. All hydrogen bonds of the closed structure open, and new ones are formed in the extended structure. For small loading rates, we found reversible rejoining of the hydrogen bond network, while the rebinding ability diminishes with increasing pulling velocity, demonstrating the feasibility of MD simulations to capture also rebinding dynamics. Calix[4]arene dimers with two longer loops (**2**) under external force display more intricate physics because the elongation proceeds in a two-step transition from a compact structure to an open one, in which complete dissociation into calix[4]arene monomers is only prevented by the mechanical locking of the loops. We present a detailed analysis of hydrogen bond breakage and show that the transition from the closed to the intermediate structure is very similar to the transition from the closed to the open structure in the tetra-loop case. The stability of the intermediate is explained in terms of the closed hydrogen bonds, which are only broken when the transition to the open structure is enforced.



INTRODUCTION

It is common knowledge that noncovalent bonds between two surfaces can produce large adhesive forces that can withstand strong mechanical load and exhibit a long lifetime in the absence of an external force. Although the individual bond might be extremely weak, the concept, adapted also by many natural systems that require strong adhesion such as a cell adhering to other cells or the substrate, only functions reliably due to the large number of parallel bonds that ensure a finite rebinding probability.^{1–3}

Under external load, individual bonds of an adhesion cluster might open but can rapidly re-form due to the fact that the neighboring molecular contacts limit the distance between the involved binding partners. Hence, reversible bonds substantially increase the lifetime of adhesion contacts, particularly at low loading rates when thermally activated dissociation might prevail.⁴

Studying reversible bond breakage in the absence of adjacent bonds and thus larger ensembles, however, requires new design principles. While nature has provided us with reversibly folding nucleic acids⁵ and proteins,⁶ a chemical approach is needed to gain full control over the energy landscape and thus the degree of reversibility to explore the rich physics of reversible bond breakage. Recently, we could show that catenanes such as those

derived from calix[4]arenes bear unprecedented control over the energy landscape and display reversible bond breakage with a minimum of chemical complexity.⁷

Interlocked structures like catenanes or rotaxanes have attracted chemists for a long time.⁸ Their potential incorporation into molecular motors or switches is an active area of current research.^{9–11} When these structures are built from cage-like molecules, they may serve as selective host systems and thus find application in molecular recognition processes. Calixarene capsules are well-known for their ability of selective complexation of ions and molecules. In particular, calix[4]arenes bearing ureas on the upper rim form dimeric capsules in the presence of an appropriate guest molecule.¹² One can thus expect that the recently synthesized catenanes consisting of calix[4]arenes are versatile building blocks for a number of applications.^{13–15} As these structures represent dimers interlocked by aliphatic loops, their mechanical properties are of utmost importance for their function. In particular, the catenane structure offers the unique possibility of switching the assembly from a closed structure

Received: March 17, 2011

Revised: April 18, 2011

Published: May 03, 2011

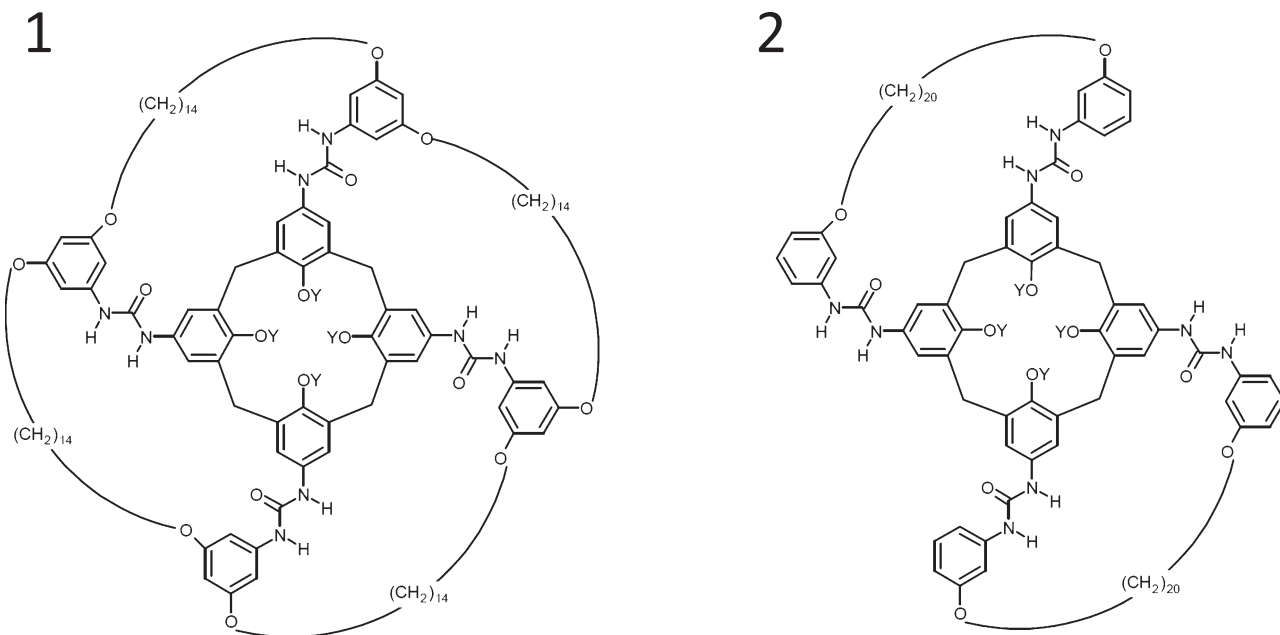


Figure 1. Structure formulas of the calix[4]arene monomers. Note the shorter loop length in the tetra-loop (1) compared to that in the bis-loop (2) system. Y = CH₃.

stabilized by hydrogen bonds to an elongated structure held together by the loops.

Experimentally, the strength and lifetime of molecular bonds such as hydrogen bond (H-bond) networks nowadays can routinely be investigated using dynamic force spectroscopy (DFS).¹⁶ Thereby, it is possible to gain detailed information about the energy landscape of biomolecules and molecular assemblies,¹⁷ and this information can in turn be used to unravel the kinetics of unfolding processes in proteins¹⁸ or also to test theorems of statistical mechanics, such as the fluctuation theorem.¹⁹ Also, the dissociation of supramolecular capsules has recently been investigated by DFS.²⁰ The experimental data usually are analyzed in terms of stochastic models based on the Kramers theory of diffusive barrier crossing in model energy landscapes.^{21–23} The lack of monomolecular reversible systems required most studies, both experimentally and theoretically, to focus on irreversible rupture under linear loading ramps.

Computer simulations have proven to be extremely useful in providing detailed insight into the mechanisms underlying conformational changes, determining reaction pathways and providing useful additional information in guiding experiments.^{24,25} MD simulations can provide valuable information about bond rupture and formation in a tunable variety of model systems and thus allow one to address a number of questions that are hard to access by other means like the quality of the approximations inherent in stochastic models or the importance of different reaction channels, for instance.

Calix[4]arene-catenanes offer the unique possibility to tune the extent of reversibility via variation of the number and the length of the loops used to interlock the dimers. Smaller loop lengths should give rise to larger recombination probabilities and, as such, should lead to systems that exhibit a more pronounced reversible behavior. Experimentally, it has been shown that the hydrogen bond dynamics in a tetra-loop calix[4]arene catenane (cf. (1) in Figure 1) is completely reversible, and the system always remain in equilibrium on the time scale of

the experiment.⁷ On the other hand, if a system interlocked by two longer loops, (2) in Figure 1, is stretched, one observes the typical hysteresis in the force versus extension curves for the pulling and the relaxing modes.^{1,4} As a function of the loading rate, the rupture force distribution moves to higher and the rejoin force distribution to smaller forces until, for very large loading rates, no rebinding can be observed and the system appears irreversible on the time scale of the experiment. In ref 7, we performed preliminary simulations in vacuo and, as to be expected for the extremely large loading rates employed in MD simulations,²⁴ found purely irreversible behavior. Furthermore, in the case of the bis-loop calix[4]arene-catenane, we identified a long-lived intermediate, which let us analyze the experimental results in terms of a stochastic model using three potential wells.

In the present paper, we present the results from MD simulations on the two different calix[4]arene-catenanes shown in Figure 1 in mesitylene solvent. In particular, we show that for the tetra-loop system, reversible rebinding of the H-bond network can be observed on the simulation time scale. Additionally, the typical hysteresis indicative of the nonequilibrium character of the dynamics behaves similar to typical experimental results as a function of the loading rate. Therefore, these chemically interesting molecules are also ideal candidates to investigate not only the rupture of the H-bond network but also the reversible re-formation and the associated nonequilibrium effects.

■ COMPUTATIONAL DETAILS

All simulations were performed using the GROMACS 4.0.7 program package²⁶ employing the force field G53AS.²⁷ In a first step, the topologies for the tetra- and bis-loop structures of the calix[4]arene-catenanes were generated with the help of the Dundee β-PRODRG2 Server,²⁸ and the topologies afterward were corrected according to the force field. (In particular, the charges have to be corrected.) For the parametrization of mesitylene molecules, we adopted the known parameters for

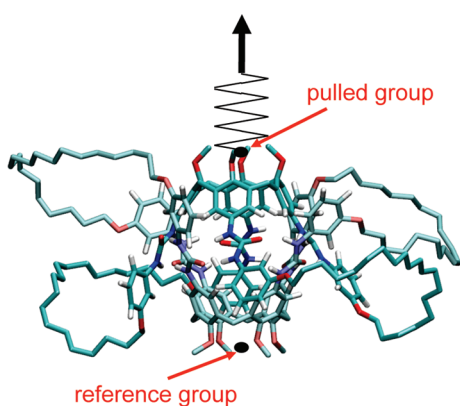


Figure 2. Stick model of the bis-loop calix[4]arene-catenane (only hydrogens bound to heteroatoms are shown) and schematic representation of the pulling simulation (definition of the reference group and the pulled group as the center of mass of the four methoxy-carbon atoms).

phenylalanine and found that the density is about 5% smaller than the experimental value. This accuracy is high enough for our purpose, in particular because mesitylene is known to be aprotic and therefore has little impact on the H-bond network dynamics. The force field parameters used in the present study are collected in the Supporting Information. In the calculations of short-ranged interactions, a cutoff of 1.4 nm was used and long-range Coulomb interactions were treated using the PME summation method,²⁹ and for the van der Waals interactions, we applied a dispersion correction.³⁰ We always used periodic boundary conditions and the simulation time-step was 2 fs which is possible because all bonds were constraint using the LINCS-algorithm.³¹ The neighbor list was updated every 10 fs. As in the experiments mentioned above,⁷ we used mesitylene as a solvent in all simulations. In the case of the tetra-loop system, the box size was 5.76 nm × 4.65 nm × 4.65 nm, and the solvent consisted of 552 mesitylene molecules (resulting in 6960 particles). For the bis-loop system, a somewhat larger box (8.23 nm × 4.60 nm × 4.60 nm) and accordingly more (791) solvent molecules (9796 particles) were used.

For the preparation of the production runs, we proceeded as follows. The first step consisted of an energy minimization for all molecules used (bis-loop and tetra-loop calix[4]arene-catenanes and mesitylene) followed by the solvation procedure. After a second energy minimization, the solvated system was equilibrated at 300 K (about 500 ps) using a velocity recycling thermostat with a time constant of 0.1 ps.³² After this, the system was coupled to a barostat (Parrinello–Rahman barostat³³ with a time constant of 2 ps and compressibility of 8.26×10^{-5} bar⁻¹), and all simulations were performed in the NPT ensemble at a temperature of 300 K and a pressure of 1 bar.

For all pulling simulations, we fixed the center of mass of the four methoxy-carbon atoms of one calix[4]arene (reference group) and applied a time-dependent harmonic pulling potential to the center of mass of the methoxy-carbon atoms of the other calix[4]arene (pulled group) (cf. Figure 2). The force experienced by the pulled group is

$$F = k(v \cdot t - z)$$

where z denotes the displacement of the pulled group from its original position and k is the spring constant of the cantilever. The pulling direction is indicated by the arrow in Figure 2. We used a force constant of $k = 830.5$ pN/nm (a typical value for MD

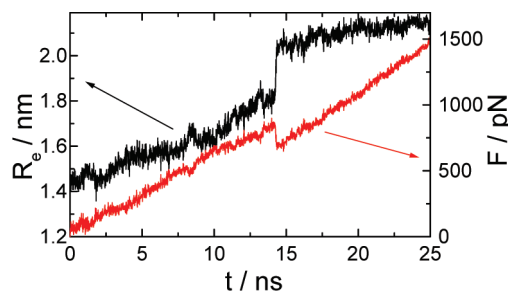


Figure 3. Measured force $F = k \cdot q$, where q is the elongation of the spring, and the molecular extension R_e for the tetra-loop system as a function of simulation time for a typical simulation run. The pulling velocity used was $v = 0.1$ nm/ns. The curves for other runs behave very similar.

simulations) and performed simulations with pulling velocities of $v = 10$, 1, and 0.1 nm/ns. In order to observe all rupture or rejoining events, we simulated the systems for 3 ns for $v = 10$ and 1 nm/ns and for 25 ns for $v = 0.1$ nm/ns. For the statistical analyses, we performed 100 simulations with $v = 10$ and 1 nm/ns and 50 simulations with $v = 0.1$ nm/ns.

For an analysis of the H-bond network, a closed H-bond was assumed to exist if the distance between the proton donor and acceptor was smaller than 0.35 nm and the H-bond angle (formed by the O–N and the O–H bonds) was smaller than 30°. The results are independent of the particular choice of these parameters in a rather wide range (distances between 0.3 and 0.4 nm and maximum angle in the range of 25–40°).

TETRA-LOOP CALIX[4]ARENE-CATENANE

Stretching the tetra-loop system with a constant pulling velocity generally results in a well-resolved step in the molecular extension along the pulling direction. This step is accompanied by the opening of a number of H-bonds and the formation of a new structure. We will discuss the details of the dynamics of the H-bond network and present an analysis of the force versus extension curves. As bond rupture and formation is a stochastic process, one has to deal with distributions of the corresponding rupture and rejoining forces, which are extracted from the analysis of a number of MD simulations.

Reversible H-Bond Network Dynamics. In Figure 3, we present results of a typical pulling trajectory. Here, we used a pulling velocity of $v = 0.1$ nm/ns and a spring constant $k = 830.5$ pN/nm, resulting in a loading rate of $\mu = k \cdot v = 83.05$ pN/ns, a typical value for MD simulations of rupture events.²⁴ The red curve (right axis) in Figure 3 shows the force measured at the spring. This is given by $F = k \cdot q$, where q is the elongation of the spring and the drop in F is related to a corresponding sudden decrease in q , which can be understood as follows. As the force increases, the system becomes more and more stretched, behaving harmonic to a good approximation, thus the linear increase in F . At the “critical” value of the force, the so-called rupture force F_R , the bonds open, and the molecule expands to a certain extent. This gives rise to a decrease in the tension experienced by the spring and a concomitant decrease of its elongation, resulting in the drop in force. As a measure for the molecular extension, we use the distance between the pulled group and the reference group, R_e (cf. Figure 2). This quantity is also shown in Figure 3 (black curve, left axis) and exhibits a jump-like increase at the time where the drop in force is observed. This jump is accompanied by the transition from a closed structure

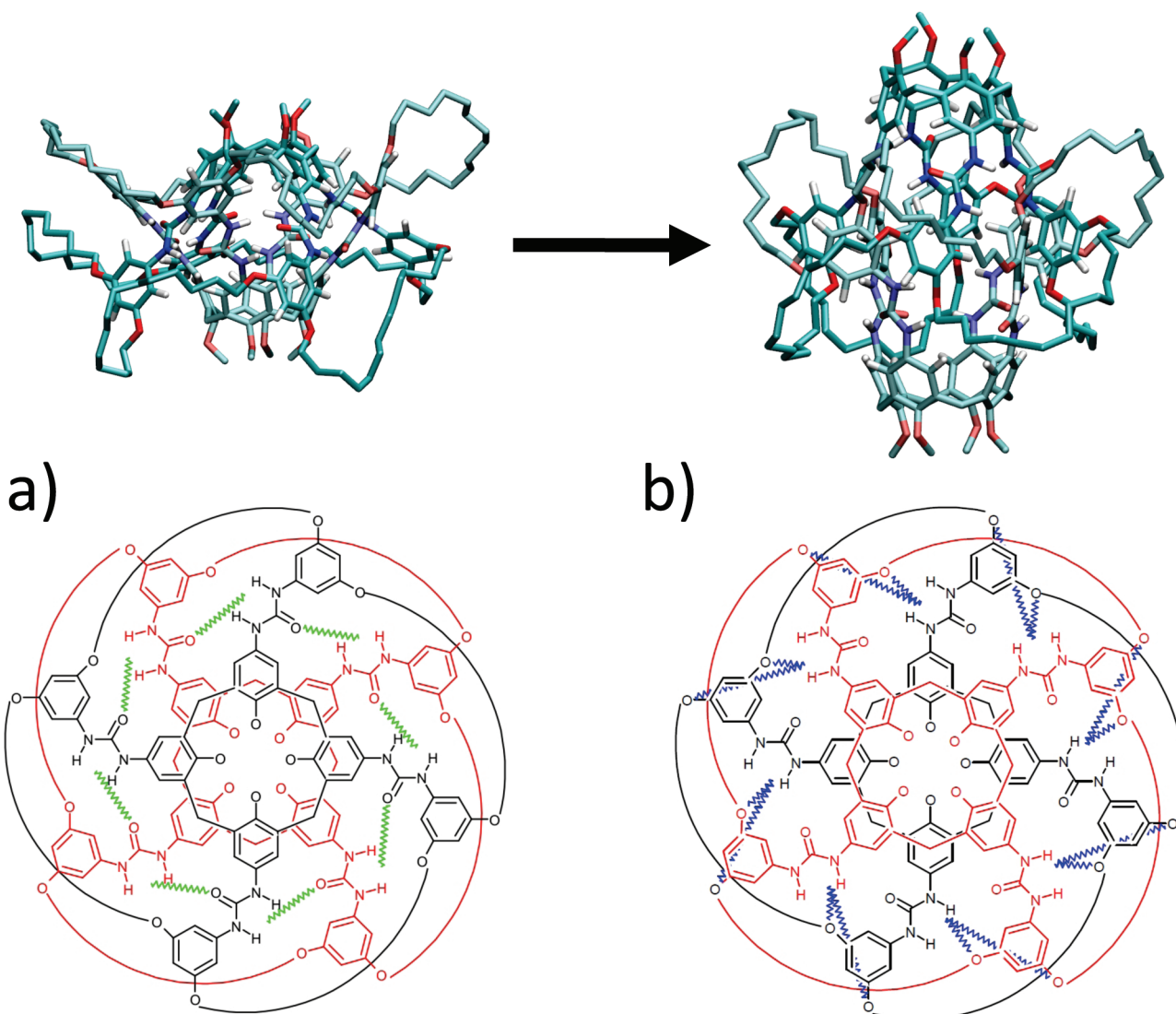


Figure 4. (Top) Examples for the configurations of the closed (C_T) ($t = 0$) and the open (O_T) ($t = 17$ ns) structures of the tetra-loop system from a pulling simulation with $v = 0.1$ nm/ns. (Bottom) Schematic representations of the tetra-loop calix[4]arene dimer. The loops consist of 14 CH_2 groups, and the endstanding CH_3 groups linked to the oxygen atoms are not shown. (a) UU bonds relevant in the C_T state, indicated in green; (b) UE bonds stabilizing the O_T state, drawn in blue.

(C_T) with $R_e(F=0) \approx 1.48$ nm to an open one (O_T) ($R_e \approx 2.0$ nm), typical examples of which are presented in Figure 4 (top).

The structures of the C_T and O_T states can very well be characterized in terms of the geometry of the networks of stabilizing H-bonds. In the C_T state, the urea groups of the two calix[4]arene monomers are arranged in a “ring-like” fashion. This geometry ideally gives rise to 16 H-bonds; for each of the eight urea pairs, there are two possible H-bonds, as indicated in Figure 4a. According to the N–O distance involved, these H-bonds can further be classified into eight “strong” (N–O distance: 0.293 nm) and eight “weak” (0.321 nm) H-bonds.^{13,34} In our simulations, we do not always observe all possible H-bonds because not all of the weak bonds are necessarily closed.

In the O_T state, all of these “urea–urea H-bonds, denoted as UU bonds in the following, are opened, and a group of new H-bonds is formed. These H-bonds are formed between one urea group and an ether group of the other monomer (cf. Figure 4b). Each urea group can, in principle, form two distinct pairs of

H-bonds, one with an ether group that is nearby and another one with an ether group somewhat further apart, giving rise to an overall number of 32 possible urea–ether H-bonds (UE bonds). The three-dimensional structure, however, shows that sterically, mainly 16 out of these will typically be formed.

As mentioned above, we are able to observe reversible rebinding of the H-bond network in the case of the tetra-loop system. In order to monitor rebinding events, in the so-called relax mode, one starts from an elongated O_T structure and linearly decreases the applied force. This means that one works with a reversed pulling velocity. For pulling velocities of 0.1 and 1 nm/ns, we find a complete restructuring of the C_T state in all simulation runs starting from the O_T state, and only for the larger velocity of 10 nm/ns is no reversible $O_T \rightarrow C_T$ transition observed. In Figure 5a, we present the results for the molecular extension and the number of H-bonds of representative simulations in the pull mode and in the relax mode. One clearly observes the $C_T \rightarrow O_T$ transition in the pull mode and the

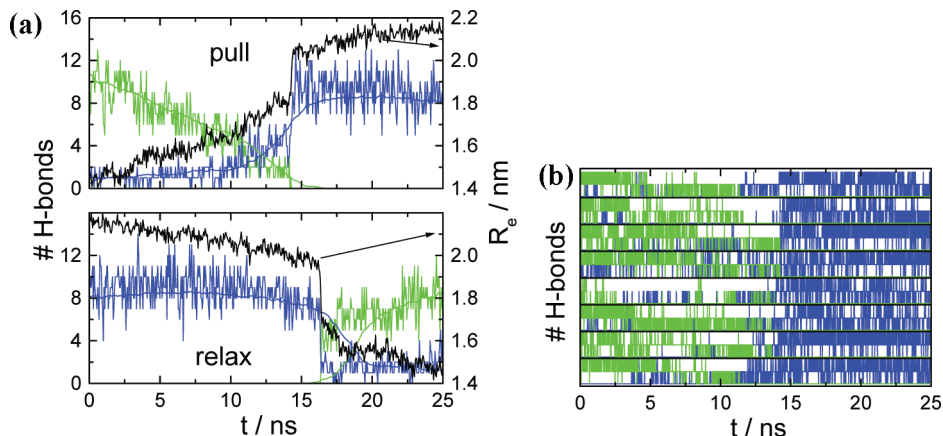


Figure 5. (a) Number of UU bonds (green), UE bonds (blue), and the molecular extension R_e (black) as a function of simulation time (pulling velocity of 0.1 nm/ns) for the tetra-loop system. (Upper panel) Pull mode ($C_T \rightarrow O_T$); (lower panel) relax mode ($O_T \rightarrow C_T$). The thin lines represent the average number of H-bonds, averaged over all 50 simulation runs. (b) Number of the individual UU (green) and UE bonds (blue) as a function of simulation time (pulling velocity of 0.1 nm/ns) in the pull mode. Each trace shows the number of H-bonds (zero, one, or two) located at one of the urea groups (cf. Figure 4). For the UE bonds, in principle, four H-bonds per urea group are conceivable (cf. Figure 4), but due to the three-dimensional structure, we never observed more than two.

reverse transition in the relax mode. The typical hysteresis effect that is observed in reversibly bonded systems^{4,5,7} is visible also in our simulation. The times for the transitions are delayed with respect to one another. While the $C_T \rightarrow O_T$ transition in the presented trajectory takes place at $t \approx 14.2 \text{ ns}$, the $O_T \rightarrow C_T$ transition in the relax mode is observed at $t \approx 16.3 \text{ ns}$ instead of $t = (25 - 14.2) \text{ ns} = 10.8 \text{ ns}$ for true equilibrium-like behavior. It is obvious that the number of the relevant H-bonds is very similar in the two modes. Furthermore, for both the UU bonds in the C_T state and the UE bonds in the O_T state, we find that the number of H-bonds appears to fluctuate around the eight strong ones.

The structure of the opening and closing of the different H-bonds is shown in more detail in Figure 5b, where the number of the individual H-bonds for each of the eight urea groups is shown as a function of time for a simulation in the pull mode. The decrease of the overall number of UU bonds as a function of time is clearly visible, and one can see that for all urea groups, apparently one weak H-bond dissociates first. Afterward, the number of UU bonds fluctuates mainly between one and zero per urea group until at the $C_T \rightarrow O_T$ transition, all UU bonds open, and the number of UE bonds increases quite rapidly. Also, their number fluctuates, and mainly two out of the four possible UE bonds are formed. These results are in agreement with the well-known stabilizing properties of the ring of H-bonds in the calix[4]arene systems, and the existence of the UE bond network in the O_T state indicates their strong mechanical resistivity. As mentioned, on the much slower experimental time scale, one observes an equilibrium between the C_T and the O_T structures. The fact that in the two states a similar number of different H-bonds stabilizes the respective conformations allows one to understand the ability of the capture of guest molecules of varying size in calix[4]arene dimers.

Rupture/Rejoin Force Distributions. We have seen above that the reversible rebinding of the calix[4]arene dimer is associated with the hysteresis typical for nonequilibrium processes. While in a MD simulation we can monitor detailed structural parameters of the system, experimentally, usually the force measured at the pulling device is recorded and plotted as a function of

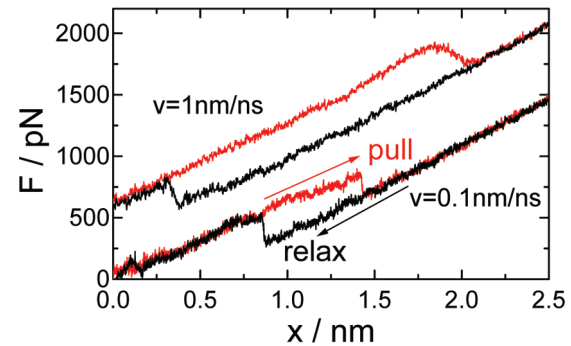


Figure 6. Representative force versus extension ($x = v \cdot t$) curves for the tetra-loop system for the pull mode (red) and the relax mode (black). The upper curves are for $v = 1 \text{ nm/ns}$ ($v = -1 \text{ nm/ns}$ in the relax mode) and are shifted by 600 pN for clarity. The lower curves are for $v = 0.1 \text{ nm/ns}$ ($v = -0.1 \text{ nm/ns}$).

the extension of the system, $x = v \cdot t$, in a so-called force versus extension (FE) curve. The typical analysis proceeds in the following way. One performs a number of pulling experiments in order to obtain enough data for a statistical analysis. From the FE curves, one extracts the rupture forces and determines their distribution function. Finally, one repeats the procedure for different values of the cantilever stiffness and/or the pulling velocity. Plotting the mean rupture force as a function of the loading rate gives the so-called force spectrum.

In the present paper, we follow the same procedure in the pull mode and the relax mode for the tetra-loop system. In Figure 6, we show typical FE curves for simulations in the pull mode (red) and in the relax mode (black) for pulling velocities of 1 and 0.1 nm/ns . These curves show the typical behavior for reversible bond breaking as observed, for instance, in Brownian dynamics simulations using a simple double-well potential,⁴ but they are also reminiscent of what is observed experimentally in the reversible unfolding of RNA hairpins.⁵ The fact that the system is pulled out of equilibrium is clearly demonstrated by the hysteresis, which is more pronounced for the larger pulling velocity.⁴ It is evident that both the forces and the fluctuations

show a very similar behavior in both modes. This can be taken as an indication for a quite well-defined conformational structure in the C_T and O_T states. As one can expect already from the data presented, for a larger pulling velocity of 10 nm/ns , we hardly observed any rebinding. Obviously, the rejoining force becomes smaller for increasing v , and therefore, one often will not be able to observe a $O_T \rightarrow C_T$ transition in the relax mode.

For pulling velocities of $v = 0.1$ and 1 nm/ns , we computed the distributions of both, the rupture forces, and the rejoin forces, where the latter are defined as the value of the force immediately after the force-jump (i.e., in the C_T state). The resulting distribution is shown in Figure 7a. For the largest velocity of 10 nm/ns , we only computed the rupture force distribution (not shown).

The mean values for the rupture forces and the rejoin forces were estimated from the distribution via a Gaussian fit, and the results are presented as a force spectrum in Figure 7b. The overall behavior of the mean forces is in accord with what one expects theoretically, in particular, the increase of the mean rupture force and the decrease of the mean rejoin force with increasing loading rate.^{4,16} However, as has been observed earlier in simulations, the absolute values of the rupture forces are larger than those experimentally observed (in our case by a factor of about 10), and also, the increase of the rupture force as a function of the loading rate is much steeper than the corresponding rise at the experimentally relevant much smaller loading rates.^{24,25,35–38} For the rejoining forces, the decay is slower, but with a change from 380 to 110 pN within one decade of change in loading rate, it is stronger than that observed experimentally for the bis-loop system.⁷ However, apart from quantitative features it is obvious that the reversible nonequilibrium dynamics of the H-bond network is well monitored by our MD simulations. The fact that we expect a change in slope in the force spectrum for smaller loading rates merely means that our simulations do not allow us to determine the minimum loading rate needed for the observation of nonequilibrium effects in terms of different values for the rupture force and the rejoin force.

BIS-LOOP CALIX[4]ARENNE DIMER

We have mentioned already that in the case of the bis-loop system, no rebinding can be observed in the MD simulations. This fact is in accord with the experimental finding that reversible rebinding is observed only for loading rates smaller than $3 \times 10^4 \text{ pN/s}$.⁷ Our preliminary simulations in vacuo⁷ showed the existence of a stable intermediate, the structure of which we discuss in more detail in the present section.

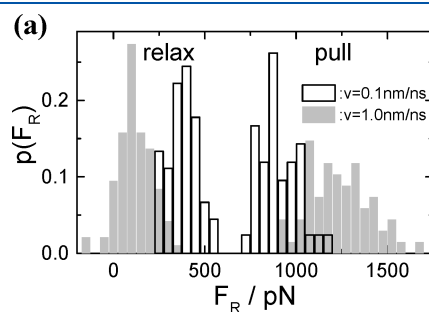


Figure 7. (a) Rupture force distribution (pull mode) and rejoin force distribution (relax mode) for the tetra-loop system for $v = 0.1$ and for 1 nm/ns (light gray). (b) Force spectrum, that is, mean rupture force (circles) and mean rejoining force (squares) as a function of the loading rate $\mu = k \cdot v$.

H-Bond Network Dynamics and Rupture Force Distributions. In Figure 8, we show results of a typical pulling trajectory of the bis-loop system, similar to the corresponding plot for the tetra-loop system (Figure 3). For times smaller than $t \approx 16.3 \text{ ns}$, that is, the time of the second rupture event, the behavior is very similar in both systems. Also for the bis-loop system, R_e changes roughly from 1.5 to 2 nm at the first step. For the next (3–4) ns, the force increases linearly with a similar slope as that before the first step, and the molecular extension hardly changes. At the second step, the force drops from roughly 800 pN to very small values, and R_e increases by about 1 nm before it further increases. It is this second transition that is absent completely in our simulations of the tetra-loop system. In addition to the pulling simulations, we performed a total number of 10 simulations in the relax mode for the same velocities, $v = 1$ and 0.1 nm/ns , starting from a representative I_B structure and the same starting from the O_B state. In neither case were we able to detect a rejoin, meaning that both transitions, $C_B \rightarrow I_B$ and $I_B \rightarrow O_B$, are irreversible on the simulation time scale.

In Figure 9, we present typical configurations from a representative simulation run. From this plot one can see that the intermediate (I_B) structure is reminiscent of the C_T state in the tetra-loop case. The open O_B -state exhibits a geometry with stretched loops.

As in the case of the tetra-loop system, in the C_B state, the urea groups of the two calix[4]arene monomers are arranged in a ring-like fashion with eight strong ($N-O$ distance: 0.286 nm) and eight weak (0.329 nm) H-bonds.³⁴ This can be anticipated from Figures 1 and because the number of urea groups is the same in the two systems. In the I_B state, the UU bonds are opened, and about 8 out of 16 possible UE bonds are formed. Note that for the bis-loop system, there are only eight ether groups available

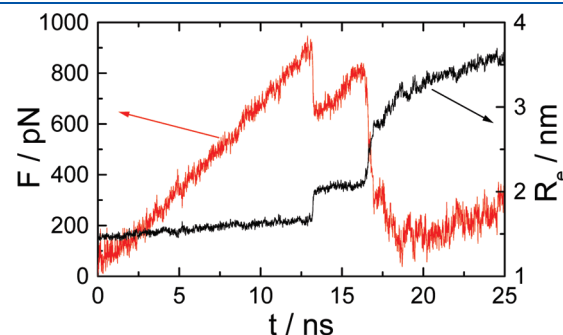
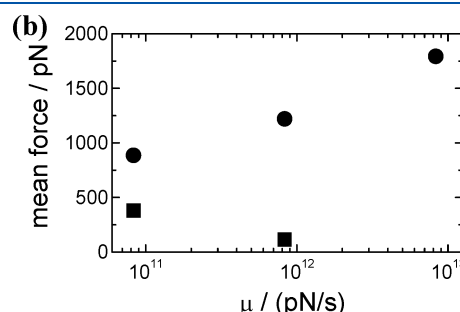


Figure 8. Measured force $F = k \cdot q$ and R_e for the bis-loop system as a function of simulation time for $v = 0.1 \text{ nm/ns}$ for a representative simulation run.



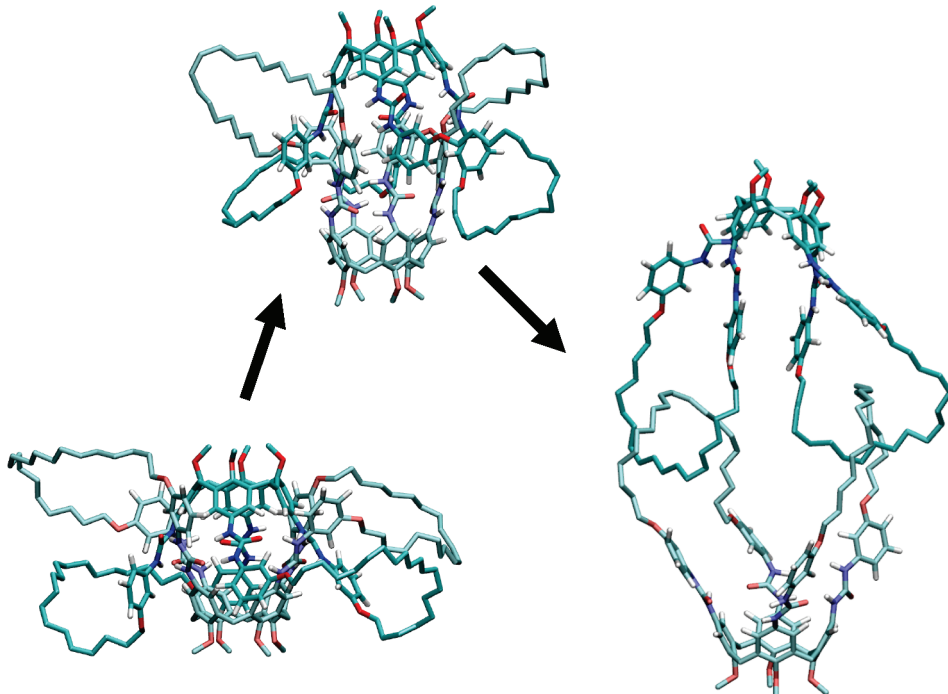


Figure 9. Examples for the configurations of the closed (C_B) ($t = 0$), the intermediate (I_B) ($t = 15$ ns), and the open (O_B) ($t = 22$ ns) structure of the bis-loop system from a pulling simulation with $v = 0.1$ nm/ns.

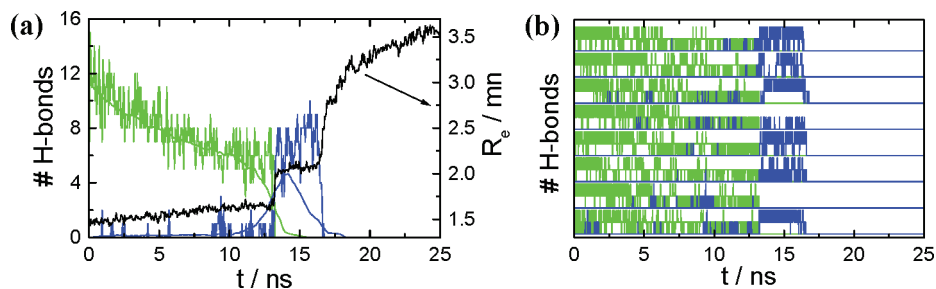


Figure 10. (a) Number of UU bonds (green), UE bonds (blue), and the molecular extension R_e (black) as a function of simulation time ($v = 0.1$ nm/ns) for the bis-loop system. The thin lines represent the average number of H-bonds, averaged over all 50 simulation runs. (b) Number of individual UU (green) and UE bonds (blue) as a function of simulation time (pulling velocity of 0.1 nm/ns). Each trace shows the number of H-bonds (zero, one, or two) located at one of the urea groups.

(cf. Figure 1). The structure of the I_B state thus is very similar to the one of the O_T state. The main difference from the tetra-loop system is in the eventual complete destruction of the H-bond network under further pulling. In the stretched O_B structure, there are no stabilizing H-bonds left, and the rupture of the dimer is prevented solely by the chemical loop structure. The strong correlation of the structures discussed to the molecular extension in a pulling simulation is shown for a representative example in Figure 10a. As in the case of the tetra-loop system, the initial decrease of the number of weak UU bonds is clearly visible. Then, there remain roughly between five and eight strong bonds that open all together at the time of the $C_B \rightarrow I_B$ transition (at about 13 ns). Immediately at that time, the UE bonds stabilizing the intermediate are formed. All of these H-bonds open again at the $I_B \rightarrow O_B$ transition, and no further H-bonds are left. In Figure 10b, the number of individual H-bonds is shown as a function of the simulation time (cf. Figure 5b for a direct comparison to the tetra-loop system). Until the I_B state decays,

the dynamics of the two systems appears very similar, showing that the calix[4]arene dimers exhibit two structures with different end-to-end distances stabilized by rings of H-bonds.

It becomes apparent from the temporal evolution of the force shown in Figure 8 that the rupture forces for the $C_B \rightarrow I_B$ transition and the $I_B \rightarrow O_B$ transition are quite similar. To quantify this behavior, we determined the rupture force distributions for both transitions. In Figure 11, we show the results obtained from all simulations for pulling velocities of 0.1 and 1 nm/ns. The values for the $C_B \rightarrow I_B$ transition ($\bar{F}_R(1\text{ nm/ns}) = 1000$ pN and $\bar{F}_R(0.1\text{ nm/ns}) = 870$ pN) are similar to those for the $I_B \rightarrow O_B$ transition ($\bar{F}_R(1\text{ nm/ns}) = 915$ pN and $\bar{F}_R(0.1\text{ nm/ns}) = 670$ pN). Given the statistical uncertainty, we do not consider the differences to be significant enough to allow for a quantitative discussion. Furthermore, the former values are in good agreement with the corresponding values found for the tetra-loop system ($\bar{F}_R(1\text{ nm/ns}) = 1200$ pN and $\bar{F}_R(0.1\text{ nm/ns}) = 890$ pN), again substantiating the similarity between the structures involved.

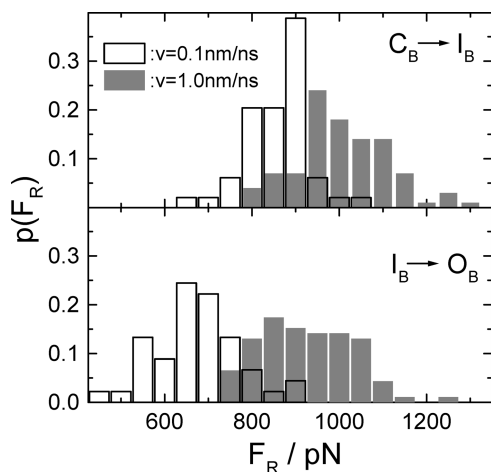


Figure 11. Rupture force distributions for the bis-loop system for $v = 0.1$ and 1.0 nm/ns .

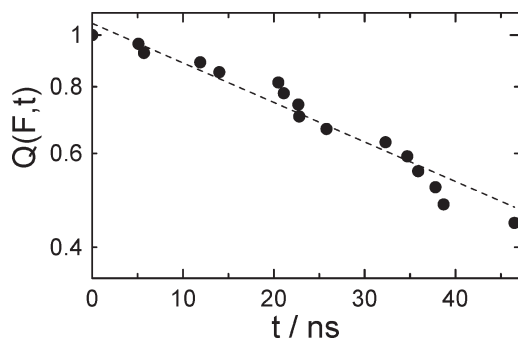


Figure 12. Fraction of molecules in the I_B state, $Q(F,t)$, as a function of time as obtained from a force-clamp simulation in which a constant force of $F = 250 \text{ pN}$ is applied along the pulling direction shown in Figure 2. The dashed line is a fit to an exponential decay with time constant $\tau \approx (59 \pm 33) \text{ ns}$.

Stability of the Intermediate. We mentioned already that we expected the intermediate I_B to be stable on experimental time scales as a result of our preliminary simulations. In the stochastic modeling of the experimental data obtained for the bis-loop calix[4]arene-catenane,⁷ we used parameters for the bare transition rates that yield a lifetime of the I_B state of $\tau \approx 4 \text{ ms}$, which appears to be a typical value accessible by DFS experiments.

In the present study, we investigated the I_B state's lifetime using a more direct route proceeding in the following way. According to the phenomenological Bell model, the lifetime of a bond is related to the applied force via a reduction in the activation energy of the bond-breaking process, $E_a(F) = E_a^0 - Fx^\ddagger$, where x^\ddagger denotes the distance between the relevant free-energy minimum and the transition state.²¹ This means that the lifetime is approximately given by

$$\begin{aligned} \tau(F, T) &\approx \tau(0, T)e^{-Fx^\ddagger/(RT)} \quad \text{with} \\ \tau(0, T) &= \tau_0 e^{E_a^0/(RT)} \end{aligned} \quad (1)$$

When applied to our situation, one expects the I_B state to be much shorter lived when a constant external force is exerted on the system than that in the force-free case. We therefore performed simulations in the so-called force-clamp mode, that is, keeping the externally applied force constant. We performed

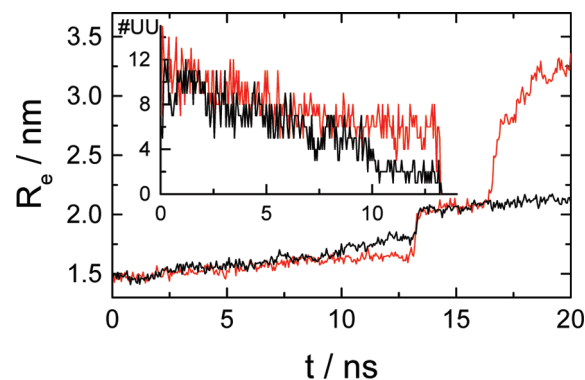


Figure 13. Molecular extension R_e measured in a representative simulation for both systems (red: bis-loop; black: tetra-loop) and $v = 0.1 \text{ nm/ns}$. In the case of the tetra-loop calix[4]arene-catenane, we subtracted 1 ns from the simulation time in order to match the rupture events. The inset shows the number of UU bonds in the closed structures.

27 simulations starting from different representative I_B state configurations and chose a value of $F = 250 \text{ pN}$. Similar to the situation in the linear-load simulations, an $I_B \rightarrow O_B$ transition is accompanied by an immediate increase in the molecular extension R_e and a concomitant drop in the number of H-bonds. Therefore, these quantities are excellent observables for identifying the transitions.

We observed 16 rupture events (transitions), and 11 molecules did not escape the I_B state in our time window of 50 ns. From the times at which these transitions take place, we can determine the fraction of molecules that still are in the I_B state, $Q(F,t)$. This quantity is plotted in Figure 12 as a function of time. Assuming a simple exponential decay law, $Q(F,t) \approx e^{-(t/\tau)}$, we can estimate the mean lifetime of the I_B state to be given by $\tau \approx 60 \text{ ns}$, with an error of about 50%. Identifying τ with the force-dependent lifetime given in eq 1, we can give approximative values for the force-free lifetime if we know the value of x^\ddagger . Estimates for such values for the unfolding of proteins are on the order of $x^\ddagger \approx 0.3 \text{ nm}$.^{39,40} We find the following values for the lifetime of the I_B state

$$\begin{aligned} \tau(x^\ddagger = 0.2 \text{ nm}) &\approx 10 \text{ ms} \\ \tau(x^\ddagger = 0.3 \text{ nm}) &\approx 4 \text{ s} \quad \tau(x^\ddagger = 0.4 \text{ nm}) \approx 1800 \text{ s} \end{aligned}$$

which means that this state might very well be relevant on experimental time scales, thus substantiating our preliminary results.⁷

■ COMMON STRUCTURES OF CALIX[4]ARENE DIMERS

When comparing the mechanical properties of the bis-loop and the tetra-loop catenanes, the most prominent difference is that a stable intermediate is only observed for the bis-loop system. The shorter loop length in the tetra-loop system prevents the existence of a structure in that all H-bonds are opened due to sterical reasons. As mentioned above, the closed structures of the bis-loop and the tetra-loop systems are very similar. Moreover, the open structure of the tetra-loop system resembles the structure of the intermediate in the bis-loop case. These structural similarities are exemplified in Figure 13, where we plot the molecular extension and the number of UU bonds obtained from

representative simulations as a function of time for both systems. It is obvious that the evolution of R_e is very similar, and the same holds for the time-dependent number of UU bonds stabilizing the closed structures. Only for times (and thus forces) in the range of the rupture event are there some minor differences. Additionally, the structural similarity between the O_T structure and the I_B structure is striking. Without showing the results, we mention that also the numbers of UE bonds, which are relevant in this case, are very similar. Of course, this structural similarity can only be observed for forces that are smaller than the rupture force for the $I_B \rightarrow O_B$ transition in the case of the bis-loop system. These results indicate that the loop structure is not very important for the caging properties of the calix[4]arene dimers. Thus, for applications in chemical host–guest systems, it appears that the details of the linkage of the calix[4]arenes can be varied to some extent. This finding is substantiated by the fact that the calix[4]arene molecules spontaneously form dimers in many “guest-capture” applications.

CONCLUSIONS

MD simulations of the forced rupture of the H-bond network of two different calix[4]arene-catenanes are presented. We observed the stochastic rupture and rebinding events of the H-bond network and found a strong dependence of the mean forces on the loading rate. In accord with earlier simulations on different systems, our rupture forces are much larger than those obtained for much smaller loading rates used experimentally. As expected from the experimental results and also from the structure of the dimers investigated, characteristic differences are observed in the dynamics. A dimer interlocked by four short loops showed true equilibrium dynamics on the experimental time scale, and in the range of loading rates investigated here, we were able to observe the nonequilibrium effects that are typical for systems exhibiting reversible dynamics, namely, a hysteresis between the FE curves in the pull and the relax modes. For the system with two long loops, these reversible nonequilibrium dynamics has been observed on the experimental time scale, and consequently, the system behaves purely irreversible on the time scale of our MD simulations. Thus, we are able to shift the transition to irreversible dynamics by about seven orders of magnitude without changing the fundamental characteristics in the H-bond network dynamics.

We presented a detailed analysis of the dynamics of the complete H-bond networks involved in both systems. In particular, we were able to clearly identify the stabilizing structures of the various states observed. The information provided by this analysis is important for an understanding of various properties of calix[4]arene-catenane systems, such as their caging ability. Interestingly, the structures that appear most relevant for cage formation appear to be very similar for the two distinct systems investigated. In both systems, we find two structures that are stabilized by rings of H-bonds, one “closed” conformation and one more open one. While there are H-bonds between the urea groups of both monomers in the closed conformation, in the latter case, a number of H-bonds between an ether group of one monomer and a urea group of the other one stabilizes the structure. From this finding, we conclude that different ways of functionalization of calix[4]arenes at the upper rim might give rise to the formation of dimers with variable structures and thus of flexible guest-capture abilities.

In accord with earlier experimental observations, we have shown that in the case of the bis-loop system with two rather long loops, a stable intermediate is formed during the pulling process. While intermediates that are only stable on short time scales often are observed in MD simulations of, for example, unfolding processes of biomolecules, we have demonstrated that the one that we observed should exhibit a lifetime long enough to be relevant for the interpretation of experimental results. We expect that applying a force-clamp will be well suited also in other systems to investigate the questions regarding lifetimes of identifiable conformational substates.

In summary, we have demonstrated that MD simulations provide invaluable information regarding the details of the chemically important H-bond network dynamics in systems exhibiting mechanical locking and thus reversible re-formation of H-bonds, which is otherwise unaccessible.

ASSOCIATED CONTENT

S Supporting Information. The force field parameters used in the MD simulations. This material is available free of charge via the Internet at <http://pubs.acs.org>.

AUTHOR INFORMATION

Corresponding Author

*E-mail: diezeman@uni-mainz.de.

ACKNOWLEDGMENT

Financial support by the Deutsche Forschungsgemeinschaft via the SFB 625 is acknowledged. We thank Gerald Hinze and Helmut Grubmüller for fruitful discussion.

REFERENCES

- (1) Seifert, U. *Europhys. Lett.* **2002**, *58*, 792.
- (2) Erdmann, T.; Schwarz, U. *Phys. Rev. Lett.* **2004**, *92*, 108102.
- (3) Weikl, T.; Asfaw, M.; Krobath, H.; Rózyckix, B.; Lipowsky, R. *Soft Matter* **2009**, *5*, 3213.
- (4) Diezemann, G.; Janshoff, A. *J. Chem. Phys.* **2008**, *129*, 084904.
- (5) Liphardt, J.; Onoa, B.; Smith, S.; Tinoco, I.; Bustamante, C. *Science* **2001**, *292*, 733.
- (6) Gebhardt, J. C. M.; Bornschlögl, T.; Rief, M. *Proc. Natl. Acad. Sci. U.S.A.* **2010**, *107*, 2013.
- (7) Janke, M.; Rudzevich, Y.; Molokanova, O.; Metzroth, T.; Mey, I.; Diezemann, G.; Marszalek, P.; Gauss, J.; Böhmer, V.; Janshoff, A. *Nat. Nanotechnol.* **2009**, *4*, 225.
- (8) Sauvage, J.-P.; Dietrich-Buchecker, C. *Molecular Catenanes, Rotaxanes, and Knots*; Wiley-VCH: Weinheim, Germany, 1999.
- (9) Pease, A.; Jeppesen, J.; Stoddart, J.; Luo, Y.; Collier, C.; Heath, J. *Acc. Chem. Res.* **2001**, *34*, 433.
- (10) Kay, E.; Leigh, D.; Zerbetto, F. *Angew. Chem., Int. Ed.* **2007**, *46*, 72.
- (11) Champin, B.; Mobian, P.; Sauvage, J.-P. *Chem. Soc. Rev.* **2007**, *36*, 358.
- (12) Rebek, J. *Chem. Commun.* **2000**, 637.
- (13) Wang, L.; Vyotsky, M.; Bogdan, A.; Bolte, M.; Böhmer, V. *Science* **2004**, *304*, 1312.
- (14) Molokanova, O.; Podoprygorina, G.; Bolte, M.; Böhmer, V. *Tetrahedron* **2009**, *65*, 7220.
- (15) Phipps, D.; Beer, P. *Tetrahedron Lett.* **2009**, *50*, 3454.
- (16) Evans, E. *Annu. Rev. Biophys. Biomol. Struct.* **2001**, *30*, 105.
- (17) Ritort, F. *J. Phys.: Condens. Matter* **2006**, *18*, R531.
- (18) Zhuang, X.; Rief, M. *Curr. Opin. Struc. Biol.* **2003**, *13*, 88.

- (19) Evans, D.; Searles, D. *Adv. Phys.* **2002**, *51*, 1529.
(20) Schröder, T.; Geisler, T.; Walhorn, V.; Schnatwinkel, B.; Anselmetti, D.; Mattay, J. *Phys. Chem. Chem. Phys.* **2010**, *12*, 10981.
(21) Bell, G. *Science* **1978**, *200*, 618.
(22) Dudko, O.; Hummer, G.; Szabo, A. *Phys. Rev. Lett.* **2006**, *96*, 108101.
(23) Dudko, O. K.; Hummer, G.; Szabo, A. *Proc. Natl. Acad. Sci. U.S.A.* **2008**, *105*, 15755.
(24) Rief, M.; Grubmüller, H. *ChemPhysChem* **2002**, *3*, 255.
(25) Sotomayor, M.; Schulten, K. *Science* **2007**, *316*, 1144.
(26) Hess, B.; Kutzner, C.; van der Spoel, D.; Lindahl, E. *J. Chem. Theory Comput.* **2008**, *4*, 435.
(27) Oostenbrink, C.; Villa, A.; Mark, A.; van Gunsteren, W. *J. Comput. Chem.* **2004**, *25*, 1656.
(28) Schüttelkopf, A. W.; van Aalten, D. M. F. *Acta Crystallogr.* **2004**, *D60*, 1355.
(29) Darden, T.; York, D.; Pedersen, L. *J. Chem. Phys.* **1993**, *98*, 10089.
(30) Allen, M.; Tildesley, D. *Computer Simulations of Liquids*; Oxford Science Publications: Oxford, U.K., 1987.
(31) Hess, B.; Bekker, H.; Berendsen, H.; Fraaije, J. *J. Comput. Phys.* **1997**, *18*, 1463.
(32) Bussi, G.; Donadio, D.; Parrinello, M. *J. Chem. Phys.* **2007**, *126*, 014101.
(33) Parrinello, M.; Rahman, A. *J. Appl. Phys.* **1981**, *52*, 7182.
(34) Vysotsky, M.; Bolte, M.; Thondorf, I.; Böhmer, V. *Chem.—Eur. J.* **2003**, *9*, 3375.
(35) Grubmüller, H.; Heymann, B.; Tavan, P. *Science* **1996**, *271*, 997.
(36) Izrailev, S.; Stepaniants, S.; Balsera, M.; Oono, Y.; Schulten, K. *Biophys. J.* **1997**, *72*, 1568.
(37) Heymann, B.; Grubmüller, H. *Chem. Phys. Lett.* **1999**, *303*, 1.
(38) Gao, M.; Lu, H.; Schulten, K. *J. Muscle Res. Cell Motil.* **2002**, *23*, 513.
(39) Li, M. *Biophys. J.* **2007**, *93*, 2644.
(40) Dougan, L.; Feng, G.; Lu, H.; Fernandez, J. *Proc. Natl. Acad. Sci. U.S.A.* **2008**, *105*, 3185.